EUROPEAN ORGANIZATION FOR NUCLEAR RESEARCH (CERN)

CERN-PH-EP/2009-002
02 February 2009

Measurement of Z-pair production in e^+e^- collisions and constraints on anomalous neutral gauge couplings

The ALEPH Collaboration*)

Abstract

The ZZ production cross section is measured from a data sample corresponding to a total integrated luminosity of 452 pb^{-1}, collected by the ALEPH experiment at LEP at centre-of-mass energies from 192 to 209 GeV. Individual cross sections, extracted at six centre-of-mass energies, are found to be in agreement with Standard Model calculations. The results are used to set limits on anomalous neutral gauge couplings.

Submitted to the Journal of High Energy Physics (JHEP)

*) See next pages for the list of authors

The ALEPH Collaboration

S. Schael

Physikalisches Institut der RWTH-Aachen, D-52056 Aachen, Germany

R. Barate, R. Brunelière, I. De Bonis, D. Decamp, C. Goy, S. Jézéquel, J.-P. Lees, F. Martin, E. Merle, M.-N. Minard, B. Pietrzyk, B. Trocmé

Laboratoire de Physique des Particules (LAPP), IN^{2}P^3-CNRS, F-74019 Annecy-le-Vieux Cedex, France

S. Bravo, M.P. Casado, M. Chmeissani, J.M. Crespo, E. Fernandez, M. Fernandez-Bosman, Ll. Garrido,[15] M. Martinez, A. Pacheco, H. Ruiz

Institut de Física d'Altes Energies, Universitat Autònoma de Barcelona, E-08193 Bellaterra (Barcelona), Spain[7]

A. Colaleo, D. Creanza, N. De Filippis, M. de Palma, G. Iaselli, G. Maggi, M. Maggi, S. Nuzzo, A. Ranieri, G. Raso,[24] F. Ruggieri, G. Selvaggi, L. Silvestris, P. Tempesta, A. Tricomi,[3] G. Zito

Dipartimento di Fisica, INFN Sezione di Bari, I-70126 Bari, Italy

X. Huang, J. Lin, Q. Ouyang, T. Wang, Y. Xie, R. Xu, S. Xue, J. Zhang, L. Zhang, W. Zhao

Institute of High Energy Physics, Academia Sinica, Beijing, The People's Republic of China[8]

D. Abbaneo, T. Barklow,[26] O. Buchmüller,[26] M. Cattaneo, B. Clerbaux,[23] H. Drevermann, R.W. Forty, M. Frank, F. Gianotti, J.B. Hansen, J. Harvey, D.E. Hutchcroft,[30], P. Janot, B. Jost, M. Kado,[2] P. Mato, A. Moutoussi, F. Ranjard, L. Rolandi, D. Schlatter, F. Teubert, A. Valassi, I. Videau

European Laboratory for Particle Physics (CERN), CH-1211 Geneva 23, Switzerland

F. Badaud, S. Dessagne, A. Falvard,[20] D. Fayolle, P. Gay, J. Jousset, B. Michel, S. Monteil, D. Pallin, J.M. Pascolo, P. Perret

Laboratoire de Physique Corpusculaire, Université Blaise Pascal, IN^{2}P^3-CNRS, Clermont-Ferrand, F-63177 Aubière, France

J.D. Hansen, J.R. Hansen, P.H. Hansen, A.C. Kraan, B.S. Nilsson

Niels Bohr Institute, 2100 Copenhagen, DK-Denmark[9]

A. Kyriakis, C. Markou, E. Simopoulou, A. Vayaki, K. Zachariadou

Nuclear Research Center Demokritos (NRCD), GR-15310 Attiki, Greece

A. Blondel,[12] J.-C. Brient, F. Machefert, A. Rougé, H. Videau

Laoratoire Leprince-Ringuet, Ecole Polytechnique, IN^{2}P^3-CNRS, F-91128 Palaiseau Cedex, France

V. Ciulli, E. Focardi, G. Parrini

Dipartimento di Fisica, Università di Firenze, INFN Sezione di Firenze, I-50125 Firenze, Italy

A. Antonelli, M. Antonelli, G. Bencivenni, F. Bossi, G. Capon, F. Cerutti, V. Chiarella, P. Laurelli, G. Mannocchi,[5] G.P. Murtas, L. Passalacqua

Laboratori Nazionali dell'INFN (LNF-INFN), I-00044 Frascati, Italy

J. Kennedy, J.G. Lynch, P. Negus, V. O'Shea, A.S. Thompson

Department of Physics and Astronomy, University of Glasgow, Glasgow G12 8QQ,United Kingdom[10]

S. Wasserbaech

Utah Valley State College, Orem, UT 84058, U.S.A.

R. Cavanaugh,[4] S. Dhamotharan,[21] C. Geweniger, P. Hanke, V. Hepp, E.E. Kluge, A. Putzer, H. Stenzel,

K. Tittel, M. Wunsch[19]

Kirchhoff-Institut für Physik, Universität Heidelberg, D-69120 Heidelberg, Germany[16]

R. Beuselinck, W. Cameron, G. Davies, P.J. Dornan, M. Girone,[1] N. Marinelli, J. Nowell, S.A. Rutherford, J.K. Sedgbeer, J.C. Thompson,[14] R. White

Department of Physics, Imperial College, London SW7 2BZ, United Kingdom[10]

V.M. Ghete, P. Girtler, E. Kneringer, D. Kuhn, G. Rudolph

Institut für Experimentalphysik, Universität Innsbruck, A-6020 Innsbruck, Austria[18]

E. Bouhova-Thacker, C.K. Bowdery, D.P. Clarke, G. Ellis, A.J. Finch, F. Foster, G. Hughes, R.W.L. Jones, M.R. Pearson, N.A. Robertson, T. Sloan, M. Smizanska

Department of Physics, University of Lancaster, Lancaster LA1 4YB, United Kingdom[10]

O. van der Aa, C. Delaere,[28] G.Leibenguth,[31] V. Lemaitre[29]

Institut de Physique Nucléaire, Département de Physique, Université Catholique de Louvain, 1348 Louvain-la-Neuve, Belgium

U. Blumenschein, F. Hölldorfer, K. Jakobs, F. Kayser, A.-S. Müller, B. Renk, H.-G. Sander, S. Schmeling, H. Wachsmuth, C. Zeitnitz, T. Ziegler

Institut für Physik, Universität Mainz, D-55099 Mainz, Germany[16]

A. Bonissent, P. Coyle, C. Curtil, A. Ealet, D. Fouchez, P. Payre, A. Tilquin

Centre de Physique des Particules de Marseille, Univ Méditerranée, IN^{2}P^3-CNRS, F-13288 Marseille, France

F. Ragusa

Dipartimento di Fisica, Università di Milano e INFN Sezione di Milano, I-20133 Milano, Italy.

A. David, H. Dietl,[32] G. Ganis,[27] K. Hüttmann, G. Lütjens, W. Männer[32], H.-G. Moser, R. Settles, M. Villegas, G. Wolf

Max-Planck-Institut für Physik, Werner-Heisenberg-Institut, D-80805 München, Germany[16]

J. Boucrot, O. Callot, M. Davier, L. Duflot, J.-F. Grivaz, Ph. Heusse, A. Jacholkowska,[6] L. Serin, J.-J. Veillet

Laboratoire de l'Accélérateur Linéaire, Université de Paris-Sud, IN^{2}P^3-CNRS, F-91898 Orsay Cedex, France

P. Azzurri, G. Bagliesi, T. Boccali, L. Foà, A. Giammanco, A. Giassi, F. Ligabue, A. Messineo, F. Palla, G. Sanguinetti, A. Sciabà, G. Sguazzoni, P. Spagnolo, R. Tenchini, A. Venturi, P.G. Verdini

Dipartimento di Fisica dell'Università, INFN Sezione di Pisa, e Scuola Normale Superiore, I-56010 Pisa, Italy

O. Awunor, G.A. Blair, G. Cowan, A. Garcia-Bellido, M.G. Green, T. Medcalf,[25] A. Misiejuk, J.A. Strong,[25] P. Teixeira-Dias

Department of Physics, Royal Holloway & Bedford New College, University of London, Egham, Surrey TW20 OEX, United Kingdom[10]

R.W. Clifft, T.R. Edgecock, P.R. Norton, I.R. Tomalin, J.J. Ward

Particle Physics Dept., Rutherford Appleton Laboratory, Chilton, Didcot, Oxon OX11 OQX, United Kingdom[10]

B. Bloch-Devaux, D. Boumediene, P. Colas, B. Fabbro, E. Lançon, M.-C. Lemaire, E. Locci, P. Perez, J. Rander, B. Tuchming, B. Vallage

CEA, DAPNIA/Service de Physique des Particules, CE-Saclay, F-91191 Gif-sur-Yvette Cedex, France[17]

A.M. Litke, G. Taylor

Institute for Particle Physics, University of California at Santa Cruz, Santa Cruz, CA 95064, USA[22]

C.N. Booth, S. Cartwright, F. Combley,[25] P.N. Hodgson, M. Lehto, L.F. Thompson

Department of Physics, University of Sheffield, Sheffield S3 7RH, United Kingdom[10]

A. Böhrer, S. Brandt, C. Grupen, J. Hess, A. Ngac, G. Prange

Fachbereich Physik, Universität Siegen, D-57068 Siegen, Germany[16]

C. Borean, G. Giannini

Dipartimento di Fisica, Università di Trieste e INFN Sezione di Trieste, I-34127 Trieste, Italy

H. He, J. Putz, J. Rothberg

Experimental Elementary Particle Physics, University of Washington, Seattle, WA 98195 U.S.A.

S.R. Armstrong, K. Berkelman, K. Cranmer, D.P.S. Ferguson, Y. Gao,[13] S. González, O.J. Hayes, H. Hu, S. Jin, J. Kile, P.A. McNamara III, J. Nielsen, Y.B. Pan, J.H. von Wimmersperg-Toeller, W. Wiedenmann, J. Wu, Sau Lan Wu, X. Wu, G. Zobernig

Department of Physics, University of Wisconsin, Madison, WI 53706, USA[11]

G. Dissertori

Institute for Particle Physics, ETH Hönggerberg, 8093 Zürich, Switzerland.

[1]Also at CERN, 1211 Geneva 23, Switzerland.

[2]Now at Fermilab, PO Box 500, MS 352, Batavia, IL 60510, USA

[3]Also at Dipartimento di Fisica di Catania and INFN Sezione di Catania, 95129 Catania, Italy.

[4]Now at University of Florida, Department of Physics, Gainesville, Florida 32611-8440, USA

[5]Also IFSI sezione di Torino, INAF, Italy.

[6]Also at Groupe d'Astroparticules de Montpellier, Université de Montpellier II, 34095, Montpellier, France.

[7]Supported by CICYT, Spain.

[8]Supported by the National Science Foundation of China.

[9]Supported by the Danish Natural Science Research Council.

[10]Supported by the UK Particle Physics and Astronomy Research Council.

[11]Supported by the US Department of Energy, grant DE-FG0295-ER40896.

[12]Now at Departement de Physique Corpusculaire, Université de Genève, 1211 Genève 4, Switzerland.

[13]Also at Department of Physics, Tsinghua University, Beijing, The People's Republic of China.

[14]Supported by the Leverhulme Trust.

[15]Permanent address: Universitat de Barcelona, 08208 Barcelona, Spain.

[16]Supported by Bundesministerium für Bildung und Forschung, Germany.

[17]Supported by the Direction des Sciences de la Matière, C.E.A.

[18]Supported by the Austrian Ministry for Science and Transport.

[19]Now at SAP AG, 69185 Walldorf, Germany

[20]Now at Groupe d' Astroparticules de Montpellier, Université de Montpellier II, 34095 Montpellier, France.

[21]Now at BNP Paribas, 60325 Frankfurt am Mainz, Germany

[22]Supported by the US Department of Energy, grant DE-FG03-92ER40689.

[23]Now at Institut Inter-universitaire des hautes Energies (IIHE), CP 230, Université Libre de Bruxelles, 1050 Bruxelles, Belgique

[24]Now at Dipartimento di Fisica e Tecnologie Relative, Università di Palermo, Palermo, Italy.

[25]Deceased.

[26]Now at SLAC, Stanford, CA 94309, U.S.A

[27]Now at CERN, 1211 Geneva 23, Switzerland

[28]Research Fellow of the Belgium FNRS

[29]Research Associate of the Belgium FNRS

[30]Now at Liverpool University, Liverpool L69 7ZE, United Kingdom

[31]Supported by the Federal Office for Scientific, Technical and Cultural Affairs through the Interuniversity Attraction Pole P5/27

[32]Now at Henryk Niewodniczanski Institute of Nuclear Physics, Polish Academy of Sciences, Cracow, Poland

1 Introduction

In the last phase of LEP, the accelerator reached centre-of-mass energies well above the Z-pair production threshold. Within the Standard Model the $e^+e^- \to ZZ \to f_1\bar{f}_1f_2\bar{f}_2$ four-fermion process is described by *crab* Feynman diagrams (Fig. 1). In this framework, the $e^+e^- \to ZZ$ resonant cross section can be expressed in terms of two diagrams, called *NC2* diagrams [1], corresponding to the example shown in Fig. 1 and to the same graph with the final-state indices inverted ($1 \leftrightarrow 2$). Anomalous neutral ZZZ or ZZγ^* couplings introduce additional diagrams, modifying the Standard Model differential cross section.

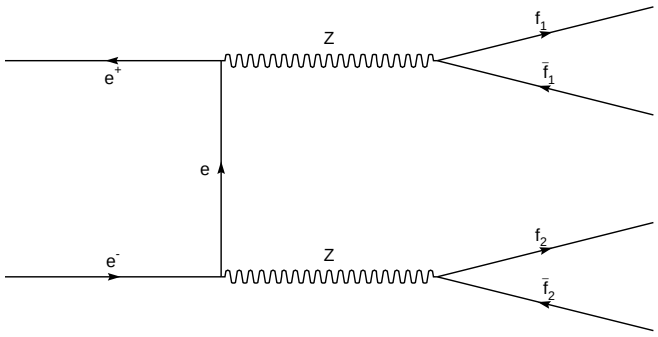

Figure 1: Example of *crab* Feynman diagram for the $e^+e^- \to ZZ$ four-fermion process.

This paper describes the measurement of the Z-pair production cross section in e^+e^- collisions with the ALEPH detector at LEP, for centre-of-mass (CM) energies from 192 to 209 GeV. Previously published results [2] were based on the data collected at CM energies of 183 and 189 GeV. The ZZ events are identified in various final states arising from Z decays into leptons, neutrinos and hadrons. The analysis closely follows the methods presented in the previous publication. The data from 183 to 209 GeV are combined to set limits on anomalous neutral gauge couplings.

The new data sample corresponds to a total integrated luminosity of 452 pb^{-1}. The results presented here are given for six different CM energies. For the last year of data taking, as the CM energy was increased in small steps, the dataset was split into two subsamples, the first integrating data at energies from 202.5 GeV to 205.5 GeV, and the second including all data taken at energies above 205.5 GeV. The luminosity breakdown is given in Table 1.

2 The ALEPH detector

A detailed description of the ALEPH detector can be found in Ref. [3] and of its performance in Ref. [4]. Charged particles are detected in the central part, consisting of a precision silicon vertex detector, a cylindrical drift chamber and a large time projection chamber, measuring altogether up to 31 space points along the charged particle trajectories. A 1.5 T axial magnetic field is provided by a superconducting solenoidal coil. Charged particle transverse momenta are reconstructed with a $1/p_T$ resolution of

Table 1: Overview of the CM energies and corresponding integrated luminosity.

Year	Energy (GeV)	Luminosity and its total error (pb^{-1})
1999	191.58	28.9 ± 0.1
	195.52	79.9 ± 0.4
	199.52	86.3 ± 0.4
	201.62	41.9 ± 0.2
2000	204.86	81.4 ± 0.4
	206.53	133.2 ± 0.6

$(6 \times 10^{-4} \bigoplus 5 \times 10^{-3}/p_T)$ $(\mathrm{GeV}/c)^{-1}$. In the following, tracks are defined as charged particle trajectories reconstructed with at least four hits in the time projection chamber, originating from within a cylinder of length 20 cm and radius 2 cm coaxial with the beam and centred at the nominal collision point, and having a polar angle with respect to the beam such that $|\cos\theta| < 0.95$.

In addition to its rôle as a tracking device, the TPC also measures the specific energy loss $\mathrm{d}E/\mathrm{d}x$ by ionization. It allows electrons of momentum lower than 8 GeV/c to be separated from pions by more than three standard deviations.

Electrons (and photons) are also identified by the characteristic longitudinal and transverse developments of the associated showers in the electromagnetic calorimeter, a 22 radiation-length thick sandwich of lead planes and proportional wire chambers with fine read-out segmentation. A relative energy resolution of $0.18/\sqrt{E}$ (E in GeV) is achieved for isolated electrons and photons.

Muons are identified by their characteristic penetration pattern in the hadron calorimeter, a 1.2 m thick iron yoke interleaved with 23 layers of streamer tubes, together with two surrounding double-layers of muon chambers. In association with the electromagnetic calorimeter, the hadron calorimeter also provides a measurement of the hadronic energy with a relative resolution of $0.85/\sqrt{E}$ (E in GeV).

Jets originating from b quarks are identified with a b-tagging algorithm. A neural network combines impact parameter and secondary vertex information with other jet properties such as track multiplicity, track rapidity, and presence of leptons, to provide an estimate of the b content of a jet. The neural network provides a value for each jet (called η in this paper) which is close to one for a b jet and close to zero for other flavours.

The total visible energy is measured with an energy-flow reconstruction algorithm which combines the information from tracking detectors and calorimeters [4]. The relative resolution on the total visible energy is $0.60/\sqrt{E}$ (E in GeV) for high multiplicity final states. In addition to the total visible-energy measurement, the energy-flow reconstruction algorithm also provides a list of reconstructed objects, classified as charged particles, photons and neutral hadrons, and called *energy-flow objects* in the following. Unless otherwise specified, these energy-flow objects are the basic entities used in the present analysis.

Below polar angles of 12° and down to 34 mrad from the beam axis, the acceptance

is closed at both ends of the experiment by the luminosity calorimeter (LCAL) [5] and a tungsten-silicon calorimeter (SICAL) [6]. The dead regions between the two LCAL modules at each end are covered by pairs of scintillators. The luminosity is measured with small-angle Bhabha events with the LCAL with an uncertainty less than 0.5%.

3 Cross section definition and Monte Carlo generators

In this paper, the ZZ production cross section is defined as the *NC2* contribution to the e^+e^- four-fermion cross section. The candidate events selected in the data arise from: *(i)* the gauge-invariant set of all four-fermion production graphs yielding ZZ-like final states and their interference (the corresponding events are called *4f* events in the following); *(ii)* some background from four-fermion production graphs yielding final states not theoretically compatible with $e^+e^- \to$ ZZ production and non-four-fermion background.

As a consequence, the measured cross section has to be corrected for the expected background, for the difference between the predicted *4f* and *NC2* cross sections in the selection acceptance (labeled *4f* − *NC2* in the following) and for the *NC2* selection efficiency. The result is the measured ZZ (or *NC2*) cross section.

The *NC2* signal, and four-fermion events compatible with ZZ final states, were generated using `KoralW` 1.51 [7]. Four-fermion events provided by `KoralW` were reweighted according to *NC2* matrix elements to give *NC2*-signal events. The efficiencies used to measure the ZZ cross sections were determined from this *NC2* sample.

The `KoralW` generator was also used for WW-like four-fermion events, produced as a separate sample. These events include all single W ($We\nu$) final states and some ZZ and Zee final states. To avoid double counting, events in the ZZ sample compatible with WW-like final states were removed.

In four-fermion events, the $q\bar{q}$ final states were simulated using parton showers and hadronization as implemented in `JETSET` 7.4 [8].

Other backgrounds were simulated as follows.

- Large angle Bhabha events were produced using the program `BHWIDE` 1.01 [9].
- Dimuon, $\mu^+\mu^-$, and ditau, $\tau^+\tau^-$, events were generated using `KK` 4.14 [10]. Initial and final state radiative corrections and their interference are included. This generator was also used for $q\bar{q}$ pairs with initial state radiation. The final state radiation was however handled by `PYTHIA` 6.1 [11] in the parton shower step and interference was therefore not included.
- Two-photon interaction processes ($e^+e^- \to e^+e^- X$), referred to as $\gamma\gamma$ events, were generated with the `PHOT02` generator [12]. When X is a pair of leptons, a QED calculation was used with preselection cuts to enrich the ZZ-like selected region. When X is a multi-hadronic state, a dedicated setup of `PYTHIA` 6.1 was used to generate untagged events where the initial electrons are scattered within 12° of

the beam. The complementary tagged events where at least one of the scattered electrons can be identified in the detector were generated with HERWIG 6.2 [13].

Events were generated for all mentioned processes at six CM energies and processed through the complete chain of detector simulation and event reconstruction. The detector simulation took into account variations in the response of the apparatus from year to year.

4 Selection of Z-pair candidates

The visible ZZ final states can be classified into four channels: $\ell^+\ell^-\mathrm{X}\bar{\mathrm{X}}$, $\ell^+\ell^-\nu\bar{\nu}$, $\mathrm{q}\bar{\mathrm{q}}\nu\bar{\nu}$, $\mathrm{q}\bar{\mathrm{q}}\mathrm{q}\bar{\mathrm{q}}$. Throughout this paper, the symbol ℓ denotes an electron or muon and X denotes a quark or charged lepton. Given the important background in the four quark channel, due to WW events, it is useful to have a dedicated b-tagging analysis and further categorize the $\mathrm{q}\bar{\mathrm{q}}\mathrm{q}\bar{\mathrm{q}}$ channel following its b-jet content.

The event selection in each topology follows closely the analysis described in [2] and only a short description is given here. In particular, the $\ell^+\ell^-\mathrm{X}\bar{\mathrm{X}}$ and $\ell^+\ell^-\nu\bar{\nu}$ selections are unchanged with respect to the previous publication. For the $\mathrm{q}\bar{\mathrm{q}}\nu\bar{\nu}$ and $\mathrm{q}\bar{\mathrm{q}}\mathrm{q}\bar{\mathrm{q}}$ channels the cut analysis described in [2] is applied, with the additional use of a kinematic fit, which has been introduced to improve the separation of the ZZ signal from background. Whenever justified, selection criteria were reoptimized at each energy.

The selections are run sequentially, in order of description, and events already selected were removed, to avoid overlap.

4.1 Selection of $\ell^+\ell^-\mathrm{X}\bar{\mathrm{X}}$ final states

The $\ell^+\ell^-\mathrm{X}\bar{\mathrm{X}}$ final state is characterized by a pair of electrons or muons consistent with a Z decay. After a preselection where at least four tracks are required, together with kinematic cuts to suppress Z radiative returns, electrons and muons are identified using standard ALEPH algorithms [4]. For electrons a bremsstrahlung recovery procedure is applied to correct for energy losses. Electrons consistent with photon conversions are rejected. Pairs of opposite-sign muons or electrons are searched for. To increase efficiency, isolated tracks are also considered as lepton candidates. (A track is considered isolated if less than 5% of the total event energy is present within an angle of 10°.) Only pairs with at least one identified lepton are considered. When both are identified they should have the same flavour. The pair with the invariant mass closest to the one of the Z boson is chosen as the $\mathrm{Z} \to \ell^+\ell^-$ candidate. Photons consistent with final-state radiation are included in the calculation of the invariant mass of the pair.

The DURHAM [14] jet-clustering algorithm is applied to the event, after excluding the two lepton candidates, to cluster the remaining energy-flow objects into two jets. A jet must include at least one charged particle. To further suppress Z radiative returns, the two-jet invariant mass must exceed 15 GeV/c^2; $\mathrm{q}\bar{\mathrm{q}}$ events are removed by requiring that the sum of the transverse momenta of the leptons with respect to the nearest jet is greater than 20 GeV/c.

For events where the $\mathrm{Z} \to \ell^+\ell^-$ pair contains one non-identified lepton (isolated track), the $\mathrm{WW} \to \mathrm{q}\bar{\mathrm{q}}\ell\nu$ process constitutes an important background. To reduce this

background, the event is assumed to represent a WW semileptonic event, and the reconstructed masses of the two W candidates, m_{lept} and m_{had}, are computed. The conditions $m_{lept} + m_{had} < 150\,\mathrm{GeV}/c^2$ and $|m_{lept} - m_{had}| > 20\,\mathrm{GeV}/c^2$ need to be fulfilled to keep the event.

In this and in the following selections, consistency with the ZZ hypothesis is enforced by means of *elliptical cuts*. For the $\ell^+\ell^-\mathrm{X}\bar{\mathrm{X}}$ final state the elliptical variable r is defined as

$$r^2 = \left(\frac{m_{\ell\ell} - m_{\mathrm{Z}}}{\sigma_{m_{\ell\ell}}}\right)^2 + \left(\frac{m_{recoil} - m_{\mathrm{Z}}}{\sigma_{m_{recoil}}}\right)^2 \quad (1)$$

where $m_{\ell\ell}$ indicates the $\ell^+\ell^-$ invariant mass, m_{recoil} represents the mass of the system recoiling against the two leptons, and σ's the expected mass resolutions, as computed from the simulation. Selected events must have $r < 3$.

Summing over the six centre-of-mass energies, 34 events are selected in this channel, with 37.3 events expected from the Standard Model simulation. The expected *NC2* purity, defined as the ratio of the *NC2* yield to all processes contributing to the selected events, is $(87 \pm 10)\%$ for the $\ell^+\ell^-\mathrm{X}\bar{\mathrm{X}}$ selection. (The uncertainties on *NC2* purities quoted in this section are statistical only.) The dependence on the CM energy of the selection efficiency is mild; this holds also for the other selections described in the following. The $\ell^+\ell^-\mathrm{X}\bar{\mathrm{X}}$ selection efficiency at a CM energy of 200 GeV is 49.3%.

4.2 Selection of $\ell^+\ell^-\nu\bar{\nu}$ final states

In the $\ell^+\ell^-\nu\bar{\nu}$ channel two acollinear, opposite-sign, same-flavour leptons (electrons or muons) are required. The acollinearity is required to be larger than 2°. No other track should be present in the event. The fraction of CM energy visible in the detector at an angle larger than 30° from the beam axis is required to be between 40% and 60%. The angle between the missing momentum and the beam axis must be larger than 6.7° and the total energy not associated with leptons is required to be less than 5.6 GeV. An elliptical variable, similar to the one defined in Eq. 1, is built using the $\ell^+\ell^-$ invariant mass and the missing mass. Selected events must have $r < 1.7$. Summing over the six centre-of-mass energies, 5 events are selected in this channel, with 6.8 events expected from the Standard Model simulation. The expected *NC2* purity of the $\ell^+\ell^-\nu\bar{\nu}$ selection is $(67 \pm 15)\%$. The selection efficiency at a CM energy of 200 GeV is 24.8%.

4.3 Selection of $\mathrm{q\bar{q}}\nu\bar{\nu}$ final states

The $\mathrm{q\bar{q}}\nu\bar{\nu}$ channel is characterized by missing and visible mass consistent with the Z mass. The analysis starts with a selection that is the same as those used for earlier studies [2] and that is briefly recalled here.

More than four tracks and a total track energy exceeding 10% of the CM energy is required. To reject $\gamma\gamma \to$ hadrons events, the total energy flow at an angle larger than 30° from the beam axis is required to be larger than 25% of the CM energy. The missing transverse energy must be larger than 5% of the CM energy. To reject Z radiative return, the total longitudinal momentum must be less than 50 GeV/c and the missing mass larger than 50 GeV/c^2. The thrust axis is used to divide the event into two hemispheres, which

are required to both have nonzero energy. The acoplanarity between the two hemispheres is required to be larger than 4.5° to reject $q\bar{q}$ events accompanied by two or more photons from initial state radiation.

Semileptonic WW $\rightarrow q\bar{q}\tau\nu$ events, where the tau decays leptonically, are rejected by requiring that electrons and muons be not isolated. The case of a hadronically decaying tau is treated by clustering events into minijets (JADE algorithm [15], $y_{cut} = 10^{-4}$) and requiring that the energy of the most isolated minijet be smaller than 8 GeV. Additionally, the angle between the highest momentum track and the nearest other track must be less than 20°. To suppress events from single W and single Z production, which are typically accompanied by an electron close to the beam axis, it is required that the energy in a 12° cone around the beam line be less than 2% of the CM energy.

With respect to Ref. [2] a kinematic fit has been introduced to improve the separation of the ZZ signal from background. First, an elliptical variable similar to the one described by Eq. 1, using the di-jet mass and the missing mass, is defined. Events are selected if $r < 2.4$. These events are then subjected to a two-constraint (2C) kinematic fit, where the di-jet invariant mass is set to be equal to the Z mass (each hemisphere, as defined above from the thrust axis, is considered as a jet) and energy conservation is imposed. Events are finally selected if the probability of the kinematic fit is larger than 1%. Figure 2 shows the di-jet mass for events passing the selection.

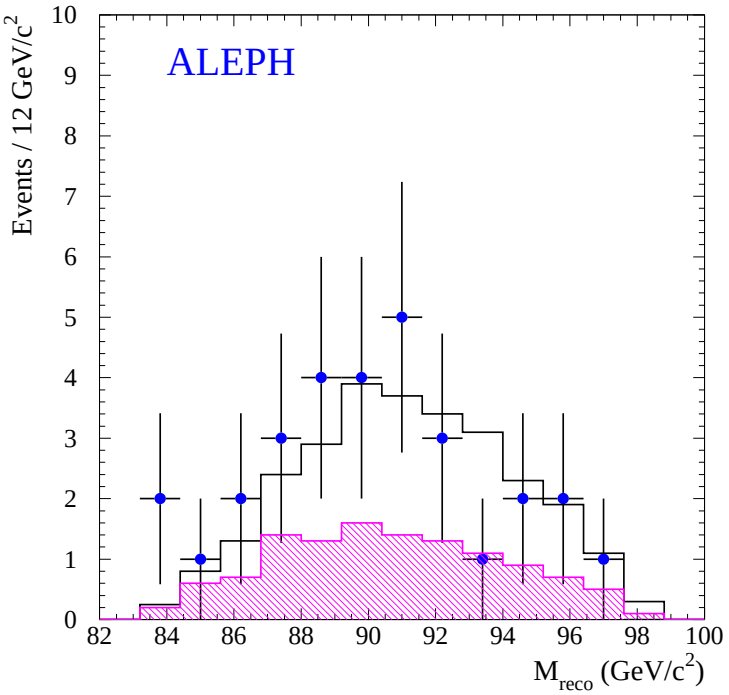

Figure 2: The di-jet invariant mass for events passing the $q\bar{q}\nu\bar{\nu}$ selection, at CM energies above 205.5 GeV. The dots correspond to the data and the histograms to the predictions. The shaded histogram shows the non-*NC2* expected events.

Summing over the six centre-of-mass energies, 100 events are selected in this channel, with 95.2 events expected from the Standard Model simulation. The expected *NC2* purity

of the $q\bar{q}\nu\bar{\nu}$ selection is $(56 \pm 5)\%$. The selection efficiency at a CM energy of 200 GeV is 44.5%.

4.4 Selection of $q\bar{q}q\bar{q}$ final states

The fully hadronic channel has the largest branching fraction, but suffers from large background from WW events. Two sub-analyses are applied: a $b\bar{b}q\bar{q}$ and a $q\bar{q}q\bar{q}$ selection. The $b\bar{b}q\bar{q}$ selection is exactly the same as the cut-based fully-hadronic b-tagging selection of Ref. [2]. The $q\bar{q}q\bar{q}$ selection has been improved with a six-constraint (6C) kinematic fit where, in addition to four-momentum conservation, two reconstructed invariant masses from the four jets are required to be equal to the Z mass.

Both analyses start with a preselection, where at least eight tracks are required and the total energy should be larger than 10% of the centre-of-mass energy. The DURHAM algorithm is used to cluster the event into four jets. Events inconsistent with a four-jet topology are suppressed by requiring a value of the three-jet/four-jet transition parameter y_{34} to be larger than 0.004. Each jet must contain at least one track. Dedicated kinematic cuts are used to suppress Z radiative returns. Two-fermion $q\bar{q}$ events are suppressed by requiring a value of the thrust less than 0.9; the sum of the four smallest angles between jets is also required to be greater than 350°.

4.4.1 b-tagged events

Events with high b content, typically due to the $b\bar{b}b\bar{b}$ topology, are selected by requiring $y_{34} > 0.02$, the sum of di-jet masses for at least one di-jet combination larger that 170 GeV/c^2, and $9.5\, y_{34} + \sum \eta_i > 3.1$. The quantity η_i is the b-tagging variable defined in Section 2 and i is the jet index. The sum is extended to the four jets.

For other events, not passing this tight b selection, the b tagging is used to set tighter di-jet mass requirements based on elliptical cuts. Defining ρ as

$$\rho^2 = \left(\frac{m_{12} + m_{34} - 2m_{\mathrm{Z}}}{\sigma_S}\right)^2 + \left(\frac{m_{12} - m_{34}}{\sigma_D}\right)^2 , \qquad (2)$$

the selection requires that at least one di-jet combination falls inside the ellipse with $\rho < 2.4$. The σ's represent the expected resolutions for the sum and the difference of di-jet masses for the correct combination, respectively. For that combination, the di-jet not containing the most poorly b-tagged jet must be compatible with a $\mathrm{Z} \to b\bar{b}$ decay: $\min(\eta_1, \eta_2) > 0.2$ and $-\log_{10}(1-\eta_1)(1-\eta_2) > 1.5$.

Summing over the six centre-of-mass energies, 42 events are selected in this sub-channel, with 46.5 events expected from the Standard Model simulation. The expected *NC2* purity of the b-tagged selection is $(69 \pm 6)\%$. The efficiency of this selection for $q\bar{q}q\bar{q}$ events with b-pairs at a CM energy of 200 GeV is 36%.

4.4.2 Non b-tagged events

Events not passing the b-tagged selection are required to satisfy $y_{34} > 0.006$. To reduce the background level, especially from hadronic W-pair decays, the 6C kinematic fit mentioned above is performed instead of applying an elliptical mass cut. For a four-jet event in the

signal hypothesis, there are in principle six possible jet combinations to form the two Z candidates. The combination with the smallest χ^2 for the kinematic fit is chosen. Events are finally selected if the χ^2 probability is greater than 0.5%. The χ^2 probability for events surviving the selection is shown in Fig. 3, for the highest CM energy point.

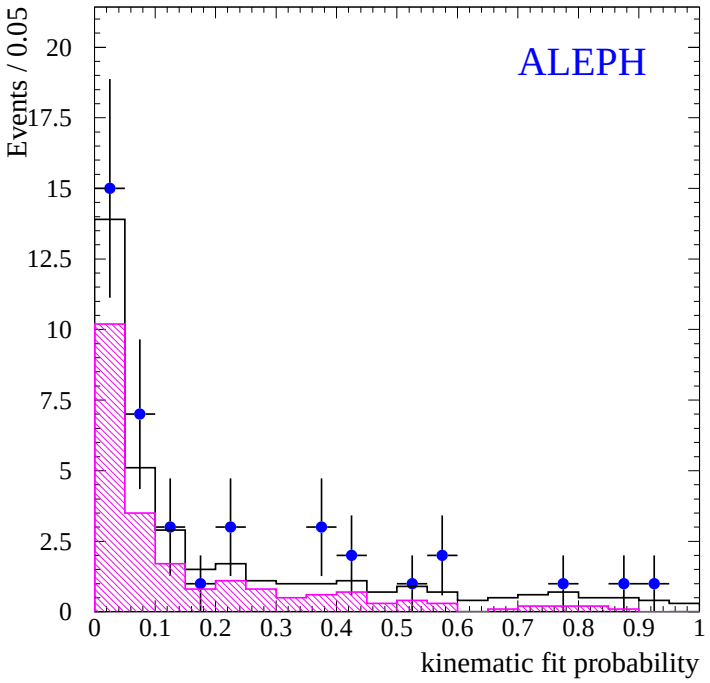

Figure 3: The kinematic fit χ^2 probability for $q\bar{q}q\bar{q}$ non b-tagged events, at CM energies above 205.5 GeV. The dots correspond to the data and the histograms to the predictions. The shaded histogram shows the non-*NC2* expected events.

Summing over the six centre-of-mass energies, 137 events are selected in this sub-channel, with 133.6 events expected from the Standard Model simulation. The expected *NC2* purity of the non-b-tagged selection is $(30 \pm 2)\%$. The efficiency of this selection for $q\bar{q}q\bar{q}$ events without b-pairs at a CM energy of 200 GeV is 24%.

5 ZZ cross section results

The *NC2* cross section is obtained from the numbers of events selected in the data, from which the expected $4f - NC2$ difference and the various backgrounds are subtracted, corrected for the *NC2* efficiencies. At each CM energy, the information from the selections in the various channels presented above is combined in a maximum likelihood fit to determine the total $e^+e^- \to ZZ$ cross section, treating as a signal the cross-contamination from events of a different ZZ final state. The Standard Model branching ratio for the Z decays is assumed in the fit. As mentioned above, the selections are not overlapping since they are run sequentially. The $4f - NC2$ plus background corrections and the efficiencies, for the six CM energies, can be found in Ref. [16]; typical values were given in the previous

section, for each selection. The measured ZZ cross sections at the various CM energies are shown in Tab. 2 and compared to theoretical predictions in Fig. 4.

Table 2: The measured $e^+e^- \to ZZ$ cross sections at the six CM energies, with statistical and systematic uncertainties.

CM Energy (GeV)	σ_{ZZ} (pb)
191.58	$0.62^{+0.40}_{-0.32} \pm 0.06$
195.52	$0.73^{+0.24}_{-0.21} \pm 0.06$
199.52	$0.91^{+0.24}_{-0.21} \pm 0.08$
201.62	$0.71^{+0.31}_{-0.26} \pm 0.08$
204.86	$1.20^{+0.27}_{-0.25} \pm 0.08$
206.53	$1.05^{+0.21}_{-0.20} \pm 0.06$

Systematic uncertainties are discussed in the next section. The ratios of the measurement to the predictions of `ZZTO` [17] and `YFSZZ` [18], at each CM energy, can be averaged to give

$$< \frac{\sigma_{ZZ}}{\sigma_{\texttt{ZZTO}}} >= 0.95 \pm 0.09\,(\text{stat.}) \pm 0.04\,(\text{syst.}) \quad (3)$$

$$< \frac{\sigma_{ZZ}}{\sigma_{\texttt{YFSZZ}}} >= 0.94 \pm 0.09\,(\text{stat.}) \pm 0.04\,(\text{syst.}) \quad (4)$$

showing that the measured ZZ cross section agrees with Standard Model calculations.

6 Systematic uncertainties

Systematic uncertainties on the cross section measurement can be due to modeling of the detector, to the description of the physical processes in the simulation, to Monte Carlo statistics and to the limited knowledge of the integrated luminosity.

The uncertainties related to detector modeling are small and typically below 1% [19, 20]. The uncertainty on the normalization of the two-fermion $q\bar{q}$ background has been extrapolated from studies performed at the Z peak and at higher energies [19], yielding a 0.8% effect. The W^+W^- cross section uncertainty has been taken as 2%; in addition the ZZ cross section has been re-evaluated by taking into account order(α) corrections to the W^+W^- process: a 0.4% effect has been found. In the simulation, the hadron fragmentation is modeled by the `JETSET` program; the fragmentation model has been changed to `HERWIG` yielding a 0.6% systematic uncertainty.

The main systematic uncertainty on this measurement is due to the limited statistics of the Monte Carlo simulation for the *4f* and *NC2* samples. The effect of the limited Monte Carlo statistics on the measured $e^+e^- \to ZZ$ *NC2* cross section has been computed with the help of a toy simulation, where the efficiencies and backgrounds in the various channels were varied according to their uncertainties, assuming Gaussian distributions. The uncertainty due to the simulated statistics amounts to 8%.

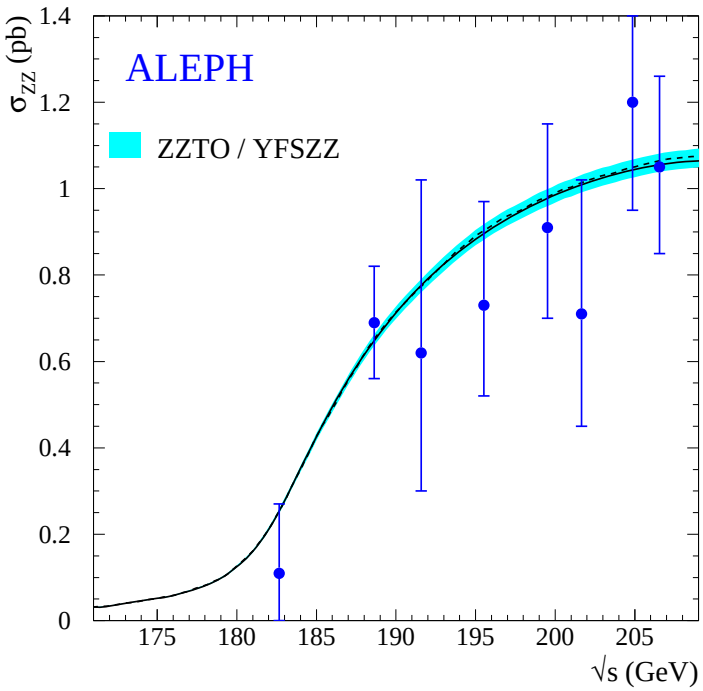

Figure 4: Measurements of the Z-pair production cross section at eight CM energies, compared to the Standard Model predictions from `YFSZZ` (solid line) and `ZZTO` (dashed line). The first two points are taken from Ref. [2]. The band represents the theoretical uncertainty on the predictions.

As a cross check of the *4f − NC2* corrections, final states corresponding to the set of *NC8* diagrams were also generated using `PYTHIA` 6.1. Compared to *NC2*, the *NC8* set includes six more graphs where one or both Z bosons are replaced by a virtual photon. Differences less than 3% with respect to the `KoralW`-based corrections were observed.

Finally, the statistical and systematic uncertainties on the knowledge of the integrated luminosity at the various CM points add an additional 0.5% systematic effect.

7 Constraints on anomalous gauge boson couplings

In the Standard Model, at the lowest order in perturbation theory, couplings between neutral gauge bosons are not expected; their presence would therefore indicate new physics. The $e^+e^- \to ZZ$ process is sensitive to possible ZZZ and ZZγ^* couplings. Following the parametrization of Ref. [21] four coupling constants (f_i^V; $i = 4, 5$; $V = Z, \gamma$) are associated to the ZZ final state; the two f_4^V's are CP-violating while the f_5^V's conserve CP.

The presence of anomalous couplings induces changes in the total cross section and in other observables, such as the Z production angle. The `YFSZZ` program [18] has been used to compute the matrix elements for different f_i^V values, and provide weights to be applied, event-by-event, to the simulated ZZ signal. The maximum likelihood fit employed to measure the total ZZ cross section has been extended to include the Z production angle, θ_Z, and the likelihood value has been studied as a function of the f_i^V couplings. To this

end, the data collected at CM energies of 183 and 189 GeV were added to the samples collected at higher energies. As an example, in Fig. 5 the measured $\cos\theta_Z$ distribution for one channel is compared to the Standard Model expectation and to one particular anomalous coupling value.

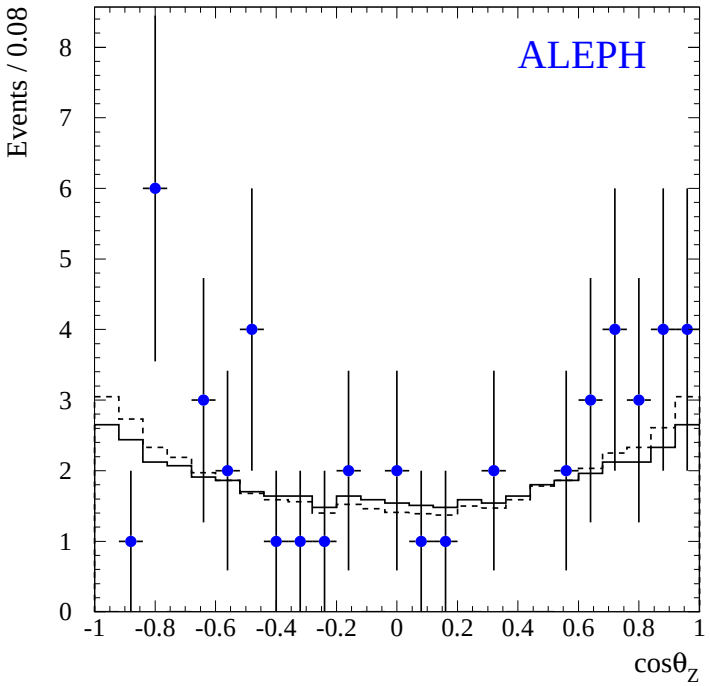

Figure 5: The measured $\cos\theta_Z$ distribution (dots) for the $\ell^+\ell^-X\bar{X}$ channel. The measurement is compared to the Standard Model expectation (solid histogram) and to one particular anomalous coupling value ($f_5^Z = +0.6$, dashed histogram).

Two kinds of likelihood fits were performed: one-parameter and two-parameter fits. In the one-parameter fits only one coupling is allowed to vary at a time, while the other three are set to zero. In the two-parameter fits both CP-violating (or CP-conserving) couplings are left free. Systematic uncertainties on the cross section measurement are included to compute the confidence levels. The uncertainty on the angular distributions has a negligible effect.

The intervals at 95% CL for the four one-parameter fits are

$$\begin{aligned} -0.321 \leq f_4^\gamma \leq +0.318 \\ -0.534 \leq f_4^Z \leq +0.534 \\ -0.724 \leq f_5^\gamma \leq +0.733 \\ -1.194 \leq f_5^Z \leq +1.190 \end{aligned}$$

The four log-likelihood curves are shown in Fig. 6: the separate contributions of the total cross sections and of the angular distributions are given. The fits are dominated by the total cross section information. The results of the two-parameter fits are given in Tab. 3.

Table 3: Results of the two-parameter fits to the CP-violating and CP-conserving couplings.

Coupling	central value	95% CL	correlation
f_4^γ	$+0.03$	$[-0.40, +0.36]$	
f_4^Z	-0.29	$[-0.60, +0.61]$	$+0.44$
f_5^γ	$+0.02$	$[-0.81, +0.79]$	
f_5^Z	-0.44	$[-1.22, +1.10]$	-0.17

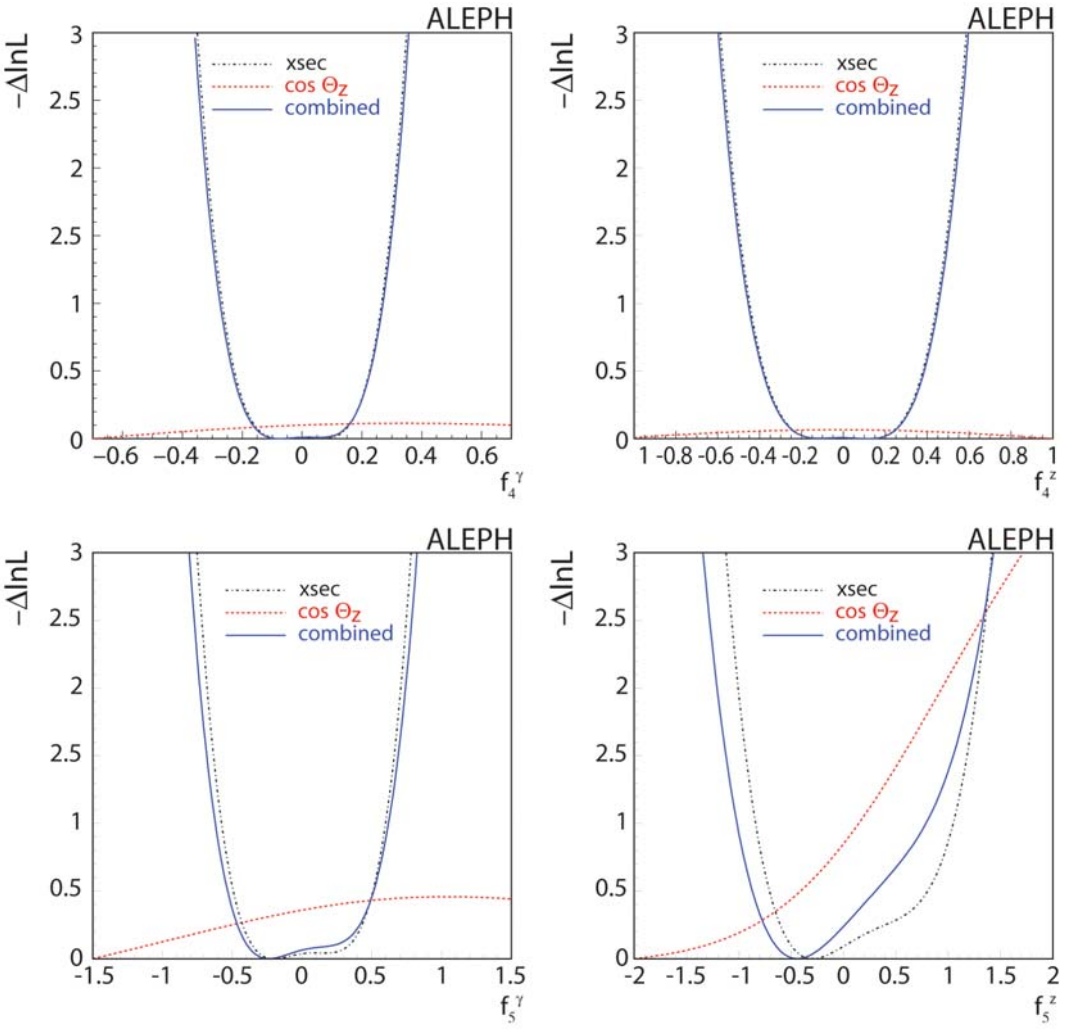

Figure 6: Log-likelihood curves for the one-parameter fits. Each figure represents the negative log-likelihood variation with respect to the minimum for one coupling, when the other three couplings are set to zero.

8 Conclusions

The Z-pair production cross section has been measured at CM energies from 192 to 209 GeV from a data sample corresponding to an integrated luminosity of 452 pb^{-1}. The

total cross sections are in agreement with the predictions of ZZTO and YFSZZ (Fig. 4). The combined ratio of the measured total cross sections to the predictions is found to be 0.94 ± 0.10 for ZZTO and 0.95 ± 0.10 for YFSZZ.

The cross section results, and the observed Z production angular distributions, have been used to set limits on anomalous neutral gauge couplings. Results of one-parameter fits to the couplings yields

$$
\begin{aligned}
-0.321 \leq f_4^\gamma \leq +0.318 \\
-0.534 \leq f_4^Z \leq +0.534 \\
-0.724 \leq f_5^\gamma \leq +0.733 \\
-1.194 \leq f_5^Z \leq +1.190
\end{aligned}
$$

at 95% CL. Similar results have been obtained by other LEP and Tevatron experiments [22].

Acknowledgments

It is a pleasure to congratulate our colleagues from the CERN accelerator divisions for the successful operation of LEP throughout the LEP2 years. We are indebted to the engineers and technicians in all our institutions for their contributions to the excellent performance of ALEPH. We wish to thank Christiane Lefevre for her help with this paper. Those of us from non-member countries thank CERN for its hospitality.

References

[1] LEP2 Workshop, CERN 96-01, Vols. 1 and 2, eds. G. Altarelli, T. Sjöstrand and F. Zwirner (1996).

[2] ALEPH Collaboration, *Measurement of the* $e^+e^- \to ZZ$ *production cross section at centre-of-mass energies of 183 and 189 GeV*, Phys. Lett. **B469** (1999) 287.

[3] ALEPH Collaboration, *ALEPH: A detector for electron-positron annihilations at LEP*, Nucl. Instrum. and Methods **A294** (1990) 121.

[4] ALEPH Collaboration, *Performance of the ALEPH detector at LEP*, Nucl. Instrum. and Methods **A360** (1995) 481.

[5] ALEPH Collaboration, *Measurement of the absolute luminosity with the ALEPH detector*, Z. Phys. **C53** (1992) 375.

[6] D.Bederede et al., *SICAL - a high precision silicon-tungsten calorimeter for ALEPH*, Nucl. Instrum. and Methods **A365** (1995) 117.

[7] S. Jadach et al., Comput. Phys. Commun. **140** (2001) 475.

[8] T. Sjöstrand, Comput. Phys. Commun. **82** (1994) 74.

[9] S. Jadach et al., Phys. Lett. **B390** (1997) 298.

[10] S. Jadach, B.F.L. Ward and Z. Wąs, Comput. Phys. Commun. **130** (2000) 260.

[11] T. Sjöstrand et al., Comput. Phys. Commun. **135** (2001) 238.

[12] J.A.M.Vermaseren, Proceedings of the IV International Workshop on Gamma Gamma Interactions, eds. G. Cochard, P. Kessler (1980).

[13] G. Corcella et al., JHEP **0101** (2001) 010.

[14] Yu.L. Dokshitzer, J. Phys. **G17** (1991) 1441.

[15] W. Bartel et al., Z. Phys. **C33** (1986) 23;
S. Bethke et al., Phys. Lett. **B213** (1988) 235.

[16] D.Fayolle, *Production de paires de* Z *et polarisation des* W *à LEP2 avec le détecteur ALEPH*, Thèse de Doctorat de l'Université Blaise Pascal, Clermont Ferrand (2002).

[17] Reports of the working groups on precision calculations for LEP2 Physics, CERN 2000-009, eds. S. Jadach, G. Passarino and R. Pittau (2000).

[18] S. Jadach, W. Placzek, B.F.L. Ward, Phys. Rev. **D56** (1997) 6939.

[19] ALEPH Collaboration, *Measurement of the* W*-pair production in* e^+e^- *collisions at centre-of-mass energies from 183 to 209 GeV*, Eur. Phys. J. **C38** (2004) 147.

[20] ALEPH Collaboration, *Observation of an excess in the search for the standard model Higgs boson in ALEPH*, Phys. Lett. **B495** (2000) 1.

[21] K. Hagiwara, K.Hikasa, R.D. Peccei and D. Zeppenfeld, Nucl. Phys. **B282** (1987) 253;
G.J. Gounaris, J.Layssac and F.M. Renard, Phys. Rev. **D62** (2000) 073012.

[22] DELPHI Collaboration, ZZ *production in* e^+e^- *interactions at* $\sqrt{s}$ *= 183-209 GeV*, Eur. Phys. J. **C30** (2003) 447;
DELPHI Collaboration, *Study of triple-gauge-boson couplings* ZZZ*,* ZZγ *and* Z$\gamma\gamma$ *at LEP*, Eur. Phys. J. **C51** (2007) 525;
L3 Collaboration, Z *boson pair-production at LEP*, Phys. Lett. **B572** (2003) 133;
OPAL Collaboration, *Study of* Z *pair production and anomalous couplings in* e^+e^- *collisions at* $\sqrt{s}$ *between 190 GeV and 209 GeV*, Eur. Phys. J. **C32** (2004) 303;
D0 Collaboration, *Search for* ZZ *and* Zγ^* *production in* $p\bar{p}$ *collisions at* $\sqrt{s}$ *= 1.96 TeV and limits on anomalous* ZZZ *and* ZZγ^* *couplings*, Phys. Rev. Lett. **100** (2008) 131801.